MARKER-LESS PREDICTION OF L5/S1 COMPRESSION LOADS DURING DYNAMIC LIFTING ACTIVITIES USING A MUSCULOSKELETAL APPROACH

Daniela S. Rubiano Blanco

EXAMINATION COMMITTEE
Dr. Ir. M. I. Refai
F.J. Wouda PhD
Prof.Dr.Ir. Massimo Sartori

UNIVERSITY OF TWENTE.

JULY 2024

Table of Contents

Marker-Less Prediction of L5/S1 Compression Loads during Dynamic lifting Activities using a musculoskeletal approach.

Daniela Sofia Rubiano Blanco[1], Mohamed Irfan Mohamed Refai [1], Massimo Sartori [1]

Abstract—**Lower back disorders are a significant health concern for industrial workers. Assessing compressive spine loads is essential for predicting low back pain (LBP). Marker-based motion tracking systems are the gold standard for human motion analysis to understand the biomechanics of the spine and its relation to LBP. However, markers placement is labor-intensive and intrusive. Existing marker-less methods often require multiple cameras and do not consider muscle forces, which are crucial for precise movement analysis. To address these limitations, this study designs and tests a marker-less approach using a single Microsoft Kinect, Nuitrack and a musculoskeletal model to compute L5/S1 joint compression loads during dynamic lifting activities. Ten participants performed different static and dynamic lifting techniques while lifting a 5kg dumbbell. OpenSim was used for inverse kinematics, dynamics, and load computations, while CEINMS handled muscle forces. The marker-less method showed strong agreement with the marker-based system, with R^2 values between 0.84 to 0.93 and RMSE ranging from 0.33 to 0.68 for inverse kinematics results. ANOVA results indicated significant differences between peak compression load estimates between the marker-less and marker-based methods ($p<0.05$). This research validates the marker-less approach for accurately computing L5/S1 forces, highlighting the significance of muscle force analysis and demonstrating its potential to be used in industrial environments, thereby improving safety.**

Index Terms—**Lower back pain, L5/S1 compression loads, Marker-less tracking, Musculoskeletal modeling, Kinect, OpenSim, CEINMS**

I. INTRODUCTION

Lower back disorders are the main health concern for industrial workers, causing about 40% of work-related musculoskeletal disorders (WMSDs) [1], [2]. Activities such as load lifting and manual materials handling (MMH) contribute to 63% of reported back injuries [3]–[6]. To improve workplace safety and reduce injury risk, it's essential to evaluate the load and moment of spine structures during lifting and MMH tasks [1], [3], [4], [7]. Studies reveal that the intervertebral joint L5/S1 is where highest loads typically occur at the lumbar spine's lower end [5], [7]. Hence, assessing compressive spine loads, commonly with lumbosacral joint moments, is crucial for predicting low back pain (LBP).

There are several methods already in use for studying the compressive spine loads. The National Institute for Occupational Safety and Health (NIOSH) offers a lifting mathematical model to estimate safe lifting limits, considering factors like load location and lifting frequency. However, it does not account for dynamic movements or individual differences [8]. Another method is by direct measurement involving sensors implanted in the intervertebral disc, providing real-time, accurate data but being invasive [9]. Furthermore, musculoskeletal models can be used to simulate movement mechanics and forces on bones, joints, and muscles. They're non-invasive, adaptable to individual differences, and useful for real-world applications [10]. Among the tools used for motion capture and musculoskeletal modeling, there are several versatile and widely used platforms available. OpenSim is an open-source server platform that provides both forward and inverse dynamics approaches [11], with various generic models tailored for specific activities. In one study, an OpenSim full-body model with detailed lumbar spine for estimating lower lumbar spine loads during symmetric and asymmetric lifting tasks was validated [12]. With this model, it is possible to study the L5/S1 kinematics and torques during lifting activities.

In addition, incorporating electromyography (EMG) data into a musculoskeletal model improves accuracy and functionality by providing precise muscle activation information [13]. EMG data ensures the model accounts for muscle activation patterns that vary between individuals leading to more personalized models [14]. CEINMS is an open-source software designed to assess internal body properties such as muscle forces, utilizing a forward dynamic modeling approach to calibrate neuromusculoskeletal computational models. It reads EMG signals from muscles and employs advanced methods for the detection, decomposition, processing, and classification of these signals [15].

To create accurate musculoskeletal models, it is first necessary to capture the subject's motion. Marker based Motion tracking systems (MTSs) are considered

[1]Neuromechanical Engineering, Department of Biomechanical Engineer ing, University of Twente, Enschede, The Netherlands

as the gold standard for human motion analysis [16]. These have been widely used across several studies [1], [3], [7], [17] to examine the L5/S1 joint moment during lifting tasks. However, its use is constrained to specialized laboratories because of their bulky size [4], [7]. Nevertheless, the process of marker placement is laborious, intrusive, susceptible to positional discrepancies caused by the operator, and vulnerable to artifacts from skin movement, particularly on soft tissues [18], [19]. Markers can dislodge from the body due to sudden accelerations or sweat, and they can also impede natural movements [19].

Multiple technologies have been explored to tackle the challenges associated with marker placement. Inertial Measurement Units (IMUs) solve complex setup and calibration required by camera systems. But, still need to be attached to the subject to measure gravity and angular rate and are prone to drift over time [20]. Another potential option is a network of RGB cameras, offering a non-invasive solution for motion capture without the need for intrusive markers. The cameras act as nodes to obtain temporally stable 3D reconstructions of multiple subjects' motion [21]. However, they demand meticulous calibration, intricate setup, substantial storage space, and high computational power [17]. Researchers have also explored the use of depth sensors, such as the Intel RealSense or the Microsoft Kinect. Some studies [8], [22] used the Kinect's skeletal model to estimate L5/S1 loads, revealing significant errors compared to traditional methods when relying on the Kinect markerless skeletal model's "spine base" location instead of the L5/S1 joint, with discrepancies of up to 33.7 cm. It highlighted the necessity for methods that minimize estimation errors while retaining the advantages of the Kinect marker less approach.

To tackle this issue and with the rise of advanced deep neural networks, various computer vision algorithms have been designed to estimate 3D human pose. OpenPose [23] is an open-source system designed to detect the human body from single images, enabling 3D pose reconstructions through the utilization of multiple 2D calibrated images [24]. Alternatively, Nuitrack, is a real time motion tracking system. It utilizes depth data to map the detected joint positions into a 3D space and offers a range of key points valuable for analyzing spine biomechanics. While it is not open source, it provides APIs to integrate with several systems and its algorithm undergoes continuous updates to improve precision and reliability.

Numerous researchers have combined networks of RGB cameras and different computer vision algorithms to evaluate L5/S1 loads during lifting tasks. One study proposed Detectron2 for 2D key-point detection, VideoPose3D for reconstructing workers' 3D poses, and a top-down inverse dynamic biomechanical approach for estimating joint angles and moments at the L5/S1 joint [2]. Another study introduced Pose2Sim, an open-source marker less kinematics workflow to connects OpenPose with OpenSim. To our knowledge only this paper has used OpenSim for skeletal modeling. It showed that a carefully designed model, when correctly scaled and constrained, can lead to accurate results from a markerless approach, despite poorly labeled joint centers and despite a low number of detected keypoints [17]. However, it didn't consider muscle forces, which can provide more accurate movement analysis and serve to identify injury-prone postures [25]. And, as the majority of the proposed methods, operates with a network of cameras, requiring additional steps to transition from 2D key-points to 3D poses. None of the papers have utilized CEINMS for computing muscle forces or attempted to gather data from moving subjects, a scenario encountered in factory settings.

Thus, the aim and scope of this study is to design, implement and test a new marker-less approach to compute L5/S1 joint compression loads during dynamic lifting activities. We utilize a single Microsoft Kinect device paired with nuitrack to reconstruct 3D poses. We have developed a process to bridge nuitrack's output with OpenSim, involving data filtering, coordinate system standardization, and translation of keypoints into markers. Subsequently, OpenSim's LFB model [12] is used to compute ID, followed by CEINMS for muscle force estimation and finally OpenSim to compute compression loads. These findings will be compared against a marker-based motion tracking system.

II. METHODS

Figure 1 illustrates our proposed pipeline for computing L5S1 compression loads. Initially, (a) the raw data from Nuitrack and Qualisys were processed separately, as described in Sections 2.B and 2.C, to account for their distinct data formats and requirements. However, following these initial steps, (b) the remaining analysis pipeline was identical for both datasets to ensure valid and reliable comparisons between the two systems.

The subsequent sections provide detailed descriptions of each component shown in figure 1.

A. Nuitrack's bridge to OpenSim

We chose to utilize Nuitrack's Key points as experimental markers for future applications within OpenSim's LFB model. Nuitrack Software presents 19 key points
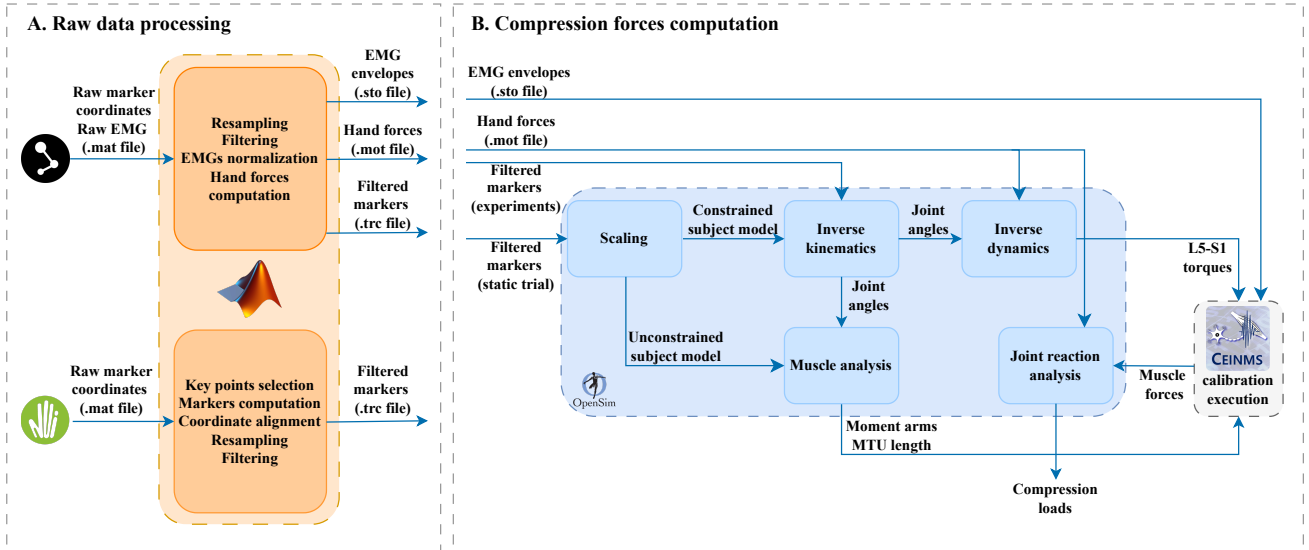
Fig. 1: Overview of the data processing pipeline used to compute L5S1 compression loads (Subsections 2.B-2.F). (A) MATLAB (orange) is used to process raw marker coordinates from Nuitrack and Qualysis separately, producing filtered marker coordinates for each, hand forces and normalized EMG envelopes. (B) OpenSim (blue) and CEINMS (grey) are then used. The process is consistent for any approach, differing only in the specific filtered marker coordinates used. Scaling uses filtered markers from a static trial to create a subject-specific model. This model and filtered markers from experiments are inputs for Inverse Kinematics, computing joint angles. These angles are inputs for Muscle Analysis, calculating moment arms and MTU lengths. Inverse Dynamics uses hand forces and joint angles to determine L5-S1 torques. CEINMS uses these torques, MTU lengths, moment arms, and EMG envelopes for calibration and execution, yielding muscle forces. Finally, Joint Reaction Analysis uses muscle and hand forces to compute compression loads. Inputs and outputs are represented by arrows, with distinct software blocks highlighted in different colors for clarity.

designed to accurately depict human poses across various scenarios, including the waist joint, neck joint, shoulders and more. However, the labeled "joints" like "Waist" lack direct anatomical significance. Consequently, We selected 15 of these key points to approximate main anatomical bony landmarks. These key points where chose to align with conventional marker placements used in the marker-based approach, ensuring comparable data for validation and consistency. They capture essential kinematic data for biomechanical analysis, enabling accurate skeletal movement reconstruction. Figure 2 shows these key points alongside the marker-based approach experimental markers.

To address the tracking limitations of Nuitrack's system, which focuses primarily on the front surface of the body, we conducted additional measurements on the subject. Specifically, we acquired the mid-thoracic anteroposterior diameter by measuring the distance from the front of the chest to the back at the level of the T7 vertebra and the xiphoid. We also measured the length of the foot from the ankle to the fifth metatarsal, and the distance between the left and right Posterior Superior Iliac Spine. These additional measurements
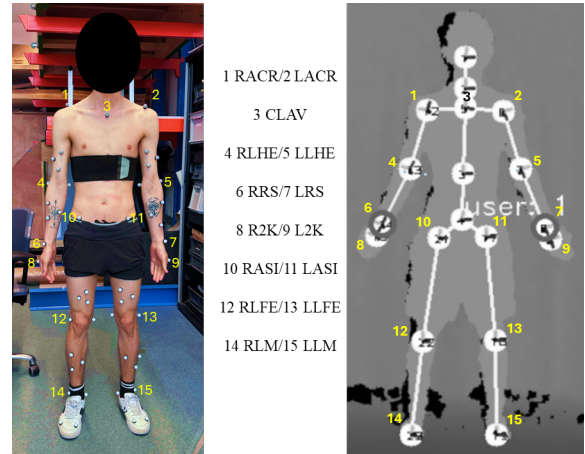

Fig. 2: Experimental markers from marker-based approach alongside the 15 selected keypoints from Nuitrack that correspond to these markers

were necessary to accurately compute markers placed on the back of the subject, such as the C7 and T10 vertebrae. Finally, cluster markers were computed by measuring the distance between keypoints at the extremities of each limb and dividing it by two. Unlike the marker-based

TABLE I: Computed experimental markers

Bony landmark	Nuitrack's keypoint	Virtual marker
Lateral Malleolus	R/L ankle	R/L LM
Fifth Metatarsal Tuberosity	R/L ankle + foot	R/L 5MT
Lateral Femoral Epicondyle	R/L knee	R/L LFE
Anterior Superior Iliac Spine	R/L hip	R/L ASI
Second metacarpophalangeal joint	R/L hand	R/L 2K
Lateral Radioulnar Sulcus	R/L wrist	R/L RS
Lateral Humeral Epicondyle	R/L elbow	R/L LHE
Acromion	R/L shoulder	R/L ACR
Clavicle	(R+L shoulder)/2	CLAV
seventh cervical vertebra	CLAV - chest depth	C7
tenth thoracic vertebra	Torso	T10
Posterior Superior Iliac Spine	Waist - (Psis/2)	L-R PSI

Note: R/L denotes the marker positioned at the identical anatomical location on both the left and right sides of the body.

approach, which uses three cluster markers per limb, we computed only one. A total of 29 experimental markers were created, in contrast to the 60 markers of the marker-based approach. Table I provides a summary of relevant computed experimental markers for Nuitrack.

Nuitrack and Opensim both follow the right-handed coordinate system convention. However, in Nuitrack, the origin (0,0,0) is established by the position of the depth sensor, in this case 3 meters away from the subject and 1.5 meters above the ground. Conversely, in OpenSim, the origin is defined by the initial standing position of the subject at the start of the trial. As a result, the origin of Nuitrack was adjusted to align with OpenSim's system. This adjustment involved subtracting 3 meters from the x-coordinate and establishing the ankles of the subject as the origin in the y-direction. Finally, a rotation of 180° was performed around the y-axis. Subsequently, the positions of other markers were determined by measuring their distance from the ankles.

The final experimental markers for the marker-less approach were subjected to filtration using a fourth-order Butterworth low-pass filter set at 6 Hz to remove noise and to ensure data consistency during frames where the body position was lost. Subsequently, the data was resampled to 50 Hz to maintain uniformity for comparison with the marker-based approach.

Finally, it is important to note that the output data collected by Nuitrack is stored in a Comma-Separated Values (.csv) file. This file format is not compatible with OpenSim. Therefore, the .csv file was used as input in MATLAB (2022a, The Mathworks, Natick, MA) to perform the to perform the processes described earlier in this section and obtain the final filtered coordinate markers. Ultimately, data was saved into a trace file (.trc), effectively bridging Nuitrack and OpenSim.

B. Marker-based approach pre-processing

MATLAB was used to pre-process the marker-based data and to get inputs for OpenSim, CEINMS and further analysis.

All signals underwent filtering using a zero-lag 2nd order Butterworth filter with a cut-off frequency of 6 Hz. Linear EMG envelopes were derived through consecutive bandpass filtering within the 30-300 Hz range, followed by full-wave rectification, and low-pass filtering with a cutoff frequency of 6 Hz. The EMG signals captured during the maximum voluntary contraction (MVC) trials were utilized to identify maximum muscle activations to subsequently normalize EMG linear envelopes. Then, all filtered signals were resampled at 50 Hz.

C. OpenSim musculoskeletal modelling

This study utilized the OpenSim lifting full-body model (LFB) [12]. The generic LFB model was adjusted to match the participant's anthropometric measurements using the scaling tool within OpenSim. Two scaled model were developed, one for the marker-less approach and one for the marker-based approach. Scaling factors were determined based on anatomical marker positions recorded during a static trial. Subsequently, the scaled model was utilized for further analyses. Inverse kinematics (IK) calculations were performed to determine joint angles at each time point using the IK toolbox in OpenSim. Additionally, inverse dynamics (ID) analysis was executed to compute L5-S1 joint torques. Hand forces were computed by calculating the shared acceleration of the hands and payload, and using the known mass which was assumed to be equally distributed between both hands. These where introduced as external forces during the ID calculations to simulate the impact of external loads. Muscle analysis was then conducted using the "Analyze" tool in OpenSim to obtain muscle-tendon unit (MTU) lengths and moment arms specific to the L5-S1 flexion-extension coordinate.

D. EMG driven modelling with CEINMS

We developed subject-specific, real-time EMG-driven musculoskeletal models using CEINMS. These models were used to estimate L5S1 joint torques and muscle forces. The required data included the inverse dynamics of the trials, normalized EMG data, L5S1 flexion-extension moment arms, and MTU lengths.

The process involved both calibration and execution phases. During the calibration phase, an uncalibrated model from OpenSim was adapted to match the subject's anatomical and physiological parameters. These parameters were determined using the normalized EMG data,

inverse dynamics of the trials, L5S1 flexion-extension moment arms, and Muscle tendon unit (MTU) lengths obtained from OpenSim. The calibration algorithm utilized one lifting repetition per lifting technique, where the subject remained stationary (see section 2.F) as a reference. Meanwhile, another model was calibrated for trials where the subject not only lifted, but also walked (see section 2.F). The execution phase was then carried out for the remaining repetitions.

E. Computing compression Loads

Finally, the OpenSim "Analyze" Tool was employed to compute the joint reaction loads, specifically focusing on compression loads. The inputs included hand forces, IK results, and muscle forces computed using CEINMS. The muscle forces were used to provide detailed internal muscle dynamics. The hand forces were introduced as external forces, ensuring accurate representation in the analysis. Additionally, the inverse IK results were used as the coordinates to supply the time history of the generalized coordinates for the model.

F. Experimental protocol

10 healthy (6 men, 4 women, age: 23 ± 1.69 years, weight: 61.6 ± 7.518 kg, height: 160.44 ± 4.52 cm) participants were enrolled in the study. None of them had a history of back or/and lower limb injuries. To ensure accurate study results regarding muscular activity, they refrained from engaging in strenuous physical activity 24 to 36 hours prior to the experiment. All of them provided written informed consent ethically approved by the Natural Sciences and Engineering Sciences Ethics Committee of the University of Twente (application number: 240249).

All participants lifted a hex dumbbell (w×d×h = 19×6×10 cm, weight = 5 kg) using two symmetric lifting (SL) techniques: Stooping (ST) and Squatting (SQ), as well as one asymmetric lifting technique: Bilateral Twisting (BT). For each of these techniques, both static (S) and dynamic (D) experiments were conducted. In the static experiment, participants performed the lifting technique while remaining in the same place. In the dynamic experiments, participants combined lifting with walking. These tasks were designed to evaluate how the marker-less approach would perform with real-life factory movements. An overview is shown in figure 3.

Before each experiment, it was necessary to perform some movements to synchronize the systems as follows:

- Movement synchronization: At the beginning of all experiments, participants were asked to take one step forward and one step backward so that Nuitrack
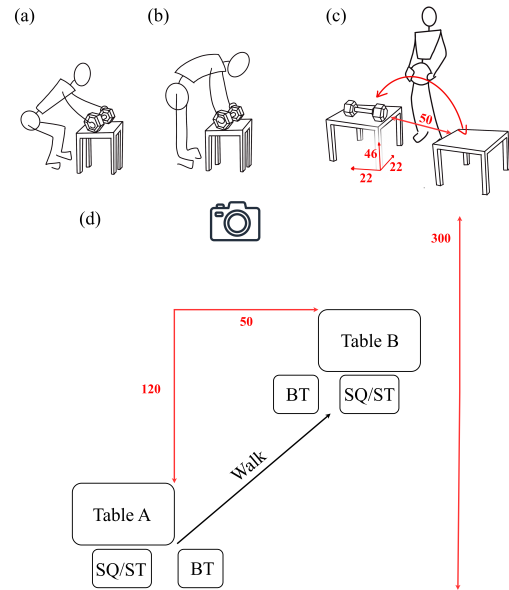

Fig. 3: Tasks to be performed (a) squat lifting (b) stoop lifting (c) bilateral lifting (d) Diagram for dynamic experiments. All measurements are given in cm

could track their movements. After this, participants were instructed to move one arm up and down. Once these preliminary steps were completed, participants proceeded with the main experiment.

For the static (S) experiments, participants were asked to perform the following:

- Symmetric lifting techniques (S-SQ and S-ST): participants were instructed to stand in front of a table (46 cm in height) with the weight positioned in front of them. They were then asked to lift the 5 kg dumbbell from the table using either the SQ or the ST, stand upright holding the weight, and place it back on the table by reversing the lifting technique. This sequence was repeated six times.
- Asymmetric lifting technique (S-BT): participants were asked to move the weight from a table positioned diagonally to the right to one positioned to the left. After standing straight, the participant had to return the weight to the starting table. These actions included one BT movement and were repeated three times.

For the dynamic (D) experiments, participants were asked to perform the following:

- Symmetric lifting techniques (D-SQ and D-ST): participants had to lift a weight from table A in front of them, walk a short distance, and place the weight on table B. This process was repeated six times.
- Asymmetric lifting technique (D-BT): participants lifted a weight from table A, positioned diagonally

to the right, walked, and placed it on table B, positioned diagonally to the left. After standing straight, participants repeated the process from left to right. These actions constituted one D-BT movement and were repeated three times.

Each participant performed both static and dynamic experiments. A complete static experiment included six SQ, six ST, and three BT trials, which was also the case for dynamic experiments. Thus, each participant performed a total of 36 liftings. Between trials, participants had a recovery period of approximately 20 seconds. The trials were divided into static and dynamic categories. The ordering of symmetric or asymmetric trials, as well as their sequence, was randomized.

G. Data collection

For the marker less method, RGB-D data was captured utilizing a Microsoft Kinect (Microsoft Corporation, Redmond, WA, USA) positioned 3.5m away from the origin, operating at a frame rate of 30 Hz. Nuitrack software (3DiVi Inc., Delaware, USA) was employed to translate the detected joint positions into a 3D spatial representation.

The Qualisys motion capture system (Qualisys Medical AB, Gothenburg, Sweden) was used as the marker-based to record the experimental sessions. Sixty spherical reflective markers were affixed to the subject's body using double-sided adhesive tape, serving to track subject kinematics. Markers placement was done as shown in Figure 2. Additionally, one marker was specifically utilized to mark the upper-left corner of the hex dumbbell (w×d×h=19×6×10 cm, weight = 5 kg) to be lifted. The 3D trajectories of both the subject's markers and the box were tracked with a 12-camera Oqus system from Qualisys, operating at a frame rate of 128 Hz.

Wireless surface EMG system from COMETA (Picolite EMG, Milan, Italy) was used to record EMG signals at a sampling rate of 2048Hz. Bipolar electrodes were placed bilaterally to record 5 dorsal muscles active during lifting and lowering activities: Longissimus Thoracis pars Thoracis (LTpT), Longissimus Thoracis pars Lumborum (LTpL), and right Iliocostalis (IL). All EMG signals, as well as the marker trajectories, were synchronized by Qualisys track manager software. Electrodes were placed as described in Moya-Esteban et al. [26].

H. Data analysis

After performing the different tests and experimental measurements, we need a reference to compare the values and understand the effectiveness of the process. We

compared the results for the compression loads obtained by the marker-less approach versus the values obtained by the marker-based approach. We used the following equation to evaluate the magnitude of the prediction errors [27].

$$RMSE = \sqrt{\frac{\sum_{i=1}^{n}(V_{val} - V_{est})^2}{n}} \qquad (1)$$

this equation represents the root mean squared error (RMSE), where V_{est} is the estimated value with the marker-less approach and V_{val} is the marker-based approach. This equation takes into consideration n samples.

By definition, the RMSE indicates how closely the experimental model (marker-less) results match the standard (marker-based) data. A lower RMSE value represents a better model, as it indicates a smaller difference from the standard. Conversely, a high RMSE means that the model significantly deviates from the standard.

In addition to the RMSE, we also evaluated the variance of the data gathered from the model, this can be achieved by studying the coefficient of determination [27], [28].

$$R^2 = 1 - \frac{\sum_{i=1}^{n}(V_{val} - V_{est})^2}{\sum_{i=1}^{n}(V_{val} - \bar{V}_{val})^2} \qquad (2)$$

Where, R^2 is the actual coefficient, (V_{val}) is the marker-based approach, (V_{est}) the marker-less approach and $(\bar{V}_{val})$ the mean. This is also done for a n number of samples.

In this case, the value of the coefficient of determination indicates how the marker-less data fits the marker-based data, and how it can be used to predict future results [29]. Hence, a high value means that the marker-less approach predictions are closely aligned with the marker-based data points, suggesting that is a good fit and accurately represents the underlying data patterns.

To assess the statistical significance of the differences in the estimated compression loads between the marker-less and marker-based motion analysis techniques, a two-way analysis of variance (ANOVA) was conducted. Prior, the data underwent Shapiro-Wilk normality testing to confirm normal distribution, ensuring the validity of the results. The analysis satisfied all the assumptions of a generalized linear model ANOVA. The model included estimation method and lifting technique as independent factors, with interaction effects examined.

III. RESULTS

A. Marker-less IK performance

Figure 4 illustrates results obtained for the average L5S1 flexion extension angles across all subjects for
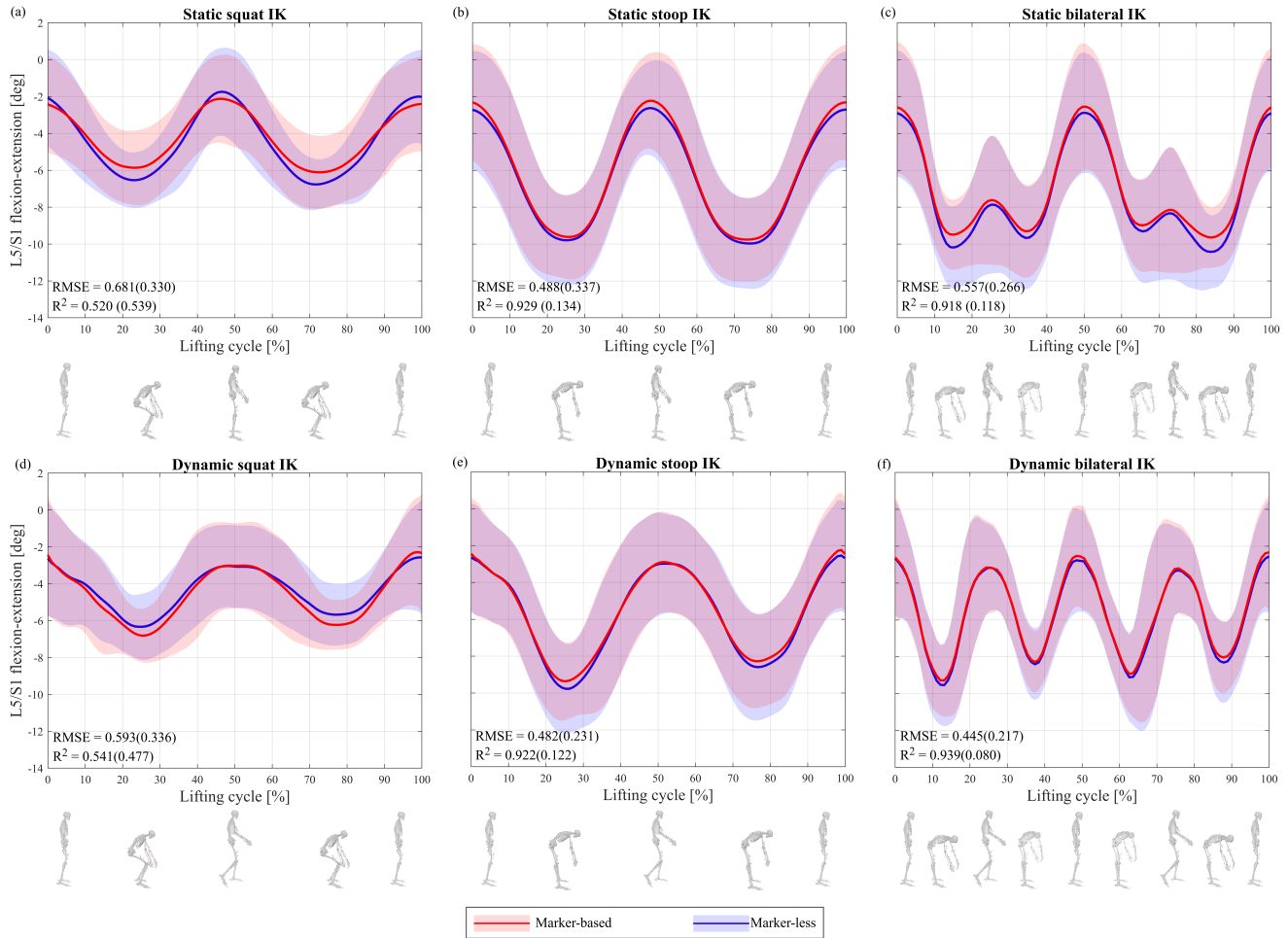
Fig. 4: Inverse kinematic results across all subjects for several lifting techniques with a 5 kg dumbbell. The techniques include S-SQ (a), S-ST (b), S-BT (c), D-SQ (d), D-ST (e), and D-BT (f). Red lines represent the marker-based approach, while blue lines represent the marker-less approach. Shaded areas indicate ± 1 standard deviation. RMSE and R_2 values as expressed as mean(standard deviation).

several lifting techniques. These techniques include S-SQ (a), S-ST (b), S-BT (c), D-SQ (d), D-ST (e), and D-BT (f), all performed with a 5 kg dumbbell. The plots depict similar patterns across static and dynamic conditions. Notably, the marker-less data exhibits slightly higher variability, as seen in the wider blue shaded regions. Despite this, the marker-less and marker-based curves align closely. Minimal phase shifts are observed, particularly in the peaks and troughs, suggesting that the marker-less data captures the timing of the lifting cycles accurately.

The R^2 values are uniformly high across all techniques, ranging from 0.520 to 0.939. The lowest R^2 values (0.520 and 0.541) are observed in the SQ technique for static and dynamic experiments. The other trials present values higher to 0.90 demonstrating particularly strong agreement with the marker-based in these cases. RMSE values range from 0.445 to 0.681, indicating the

extent of deviation between the marker-less approach and the marker-based. The lowest RMSE value (0.445) is observed in the D-BT technique, suggesting that the marker-less approach performs best in this scenario with the least error. The consistently high R^2 values indicate robust agreement, while the RMSE values show that the deviations are minimal and manageable.

B. Marker-less ID performance

Figure 5 illustrates results obtained for the average L5S1 moment (normalized to body weight) across all subjects for all lifting techniques. The shapes of the curves are quite similar across both methods, with both exhibiting peaks and troughs at corresponding phases of the lifting cycle. Generally, the marker-less method exhibits a wider shaded area, suggesting higher variability compared to the marker-based method. There are minor
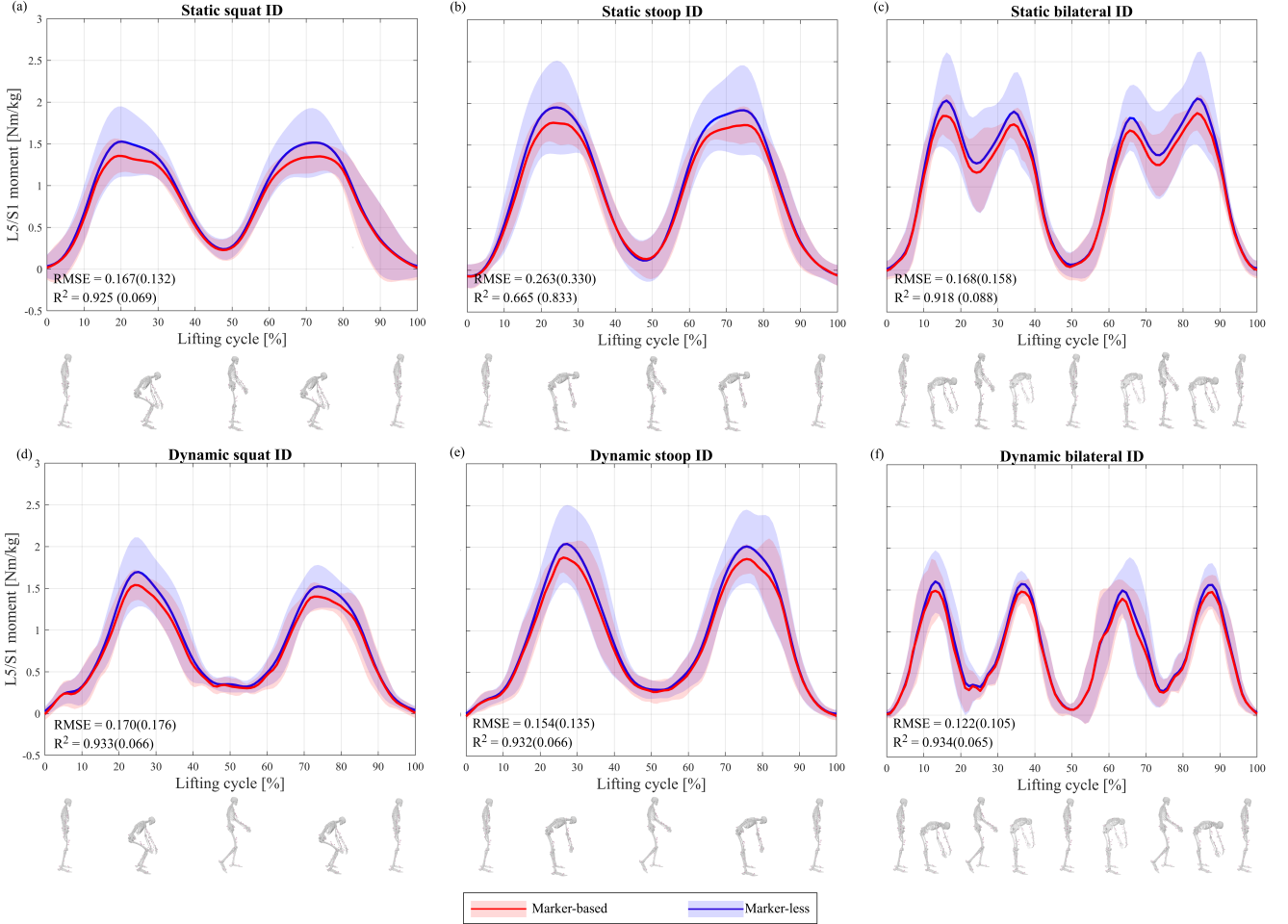
Fig. 5: Inverse dynamics results (normalized to body weight) across all subjects for several lifting techniques with a 5 kg dumbbell. The techniques include S-SQ (a), S-ST (b), S-BT (c), D-SQ (d), D-ST (e), and D-BT (f). Red lines represent the marker-based approach, while blue lines represent the marker-less approach. Shaded areas indicate $\pm$ 1 standard deviation. RMSE and R_2 values as expressed as mean(standard deviation).

phase shifts between the two methods, but overall, the curves align closely, especially in dynamic conditions.

The R^2 values are uniformly high across all techniques, ranging from 0.665 to 0.934. The lowest R^2 value (0.665) is observed in the S-ST technique, indicating a slightly lower agreement between the marker-less and marker-based methods. The other techniques R^2 values higher than 0.90, demonstrating particularly strong agreement with the marker-based method in these cases. RMSE values range from 0.122 to 0.263, indicating the extent of deviation between the marker-less approach and the marker-based. The lowest RMSE value (0.122) is observed in the D-BT technique, suggesting that the marker-less approach performs best in this scenario with the least error. The consistently high R^2 values indicate robust agreement across all techniques, while the RMSE values show that the deviations are minimal and manageable.

C. Marker-less Compression loads performance

Figure 6 illustrates results obtained for the average compression loads (expressed as times body weight) across all subjects. The curves exhibit smooth waveforms, reflecting the cyclical nature of the lifting activities, with peaks and troughs aligning closely. The shaded areas show that the marker-less data (blue) has higher variability compared to the marker-based data (red). Despite this increased variability, the overall trends and patterns between the two data sets remain consistent. Minor phase shifts are observed, particularly in the timing of peaks and troughs, indicating that while the marker-less data is slightly out of sync, it still captures the key phases of the lifting cycles reasonably well.

The R^2 values range from 0.237 to 0.832, indicating a strong correlation between the marker-less approach and the marker-based approach across all lifting techniques. The highest R^2 value is 0.832 for the D-ST technique,
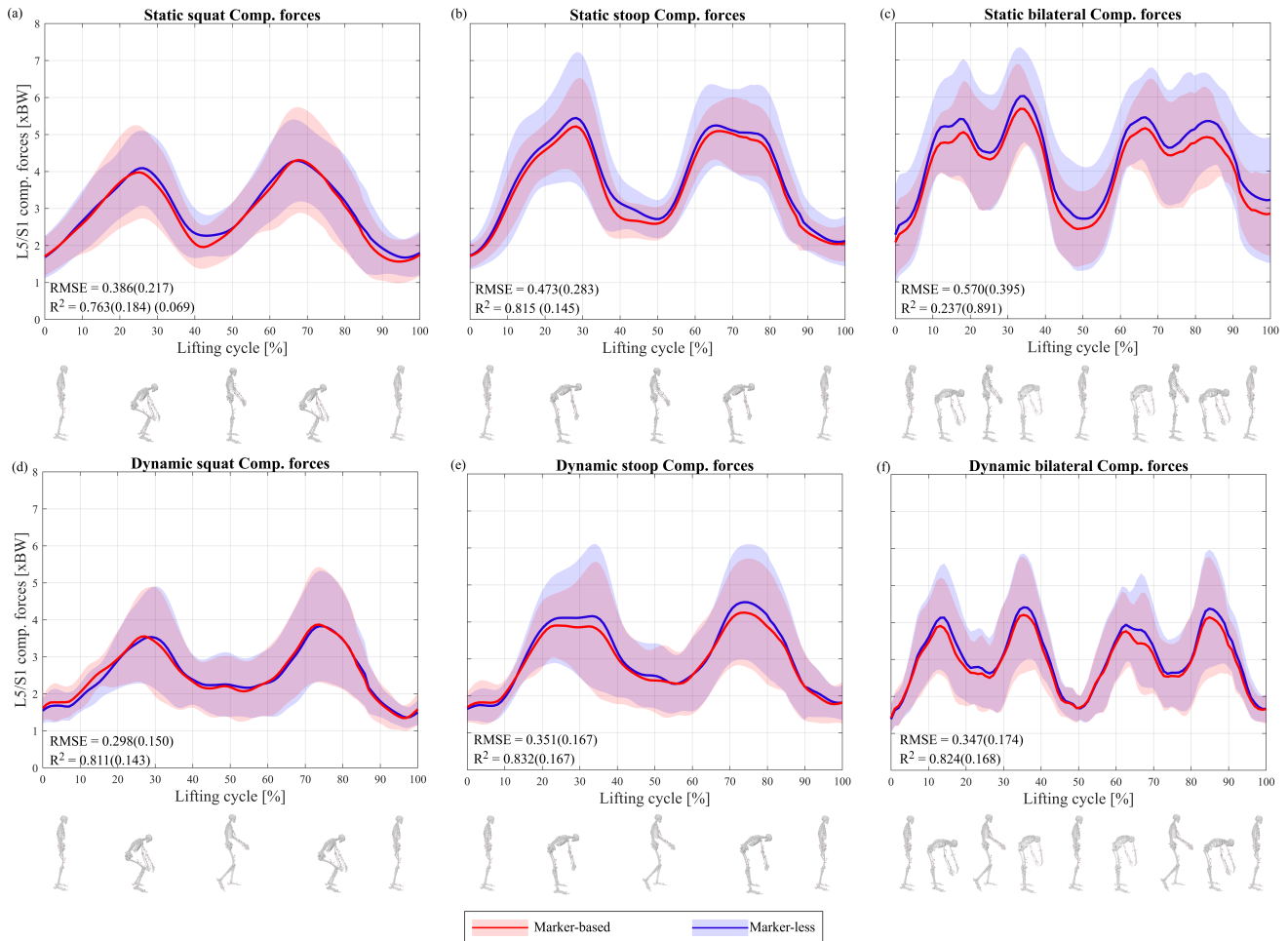
Fig. 6: Results of L5/S1 compression forces (expressed as times body weight) across all subjects for several lifting techniques with a 5 kg dumbbell. The techniques include S-SQ (a), S-ST (b), S-BT (c), D-SQ (d), D-ST (e), and D-BT (f). Red lines represent the marker-based approach, while blue lines represent the marker-less approach. Shaded areas indicate the standard deviation. RMSE and R_2 values as expressed as mean(standard deviation).

suggesting the best alignment with the marker-based approach. The lowest R^2 value is 0.237 for the S-BT technique, indicating relatively lower correlation. The RMSE values range from 0.298 to 0.57, showing varying levels of deviation between both approaches. The lowest RMSE value is 0.298 for the D-SQ technique, indicating the least deviation and highest precision. The highest RMSE value is 0.57 for the S-BT, suggesting the greatest deviation and lower precision.

Overall, the marker-less approach for ID moment measurements shows better correlation with higher R^2 values and lower RMSE, particularly in dynamic conditions. The compression load measurements also show strong correlation, with high R^2 values, but have slightly higher RMSE compared to ID moments. The IK results, while showing good correlation, have higher RMSE values than both ID moments and compression loads, indicating slightly lower precision.

D. Peak compression loads

Figure 7 illustrates the differences in L5-S1 peak compression load estimations using the marker-less approach compared to the marker-based for all lifting techniques. Talking about the static experiments, S-ST consistently shows the largest differences across most trials, particularly in trials 4, 6, and 7, while S-BT generally exhibits the smallest differences except for spikes in trials 6 and 8. For dynamic experiments, the D-ST technique demonstrates higher differences in several trials, notably 1, 4, 7, and 8, whereas D-BT shows more consistent and lower differences, with occasional peaks in trials 7 and 8.

The results of ANOVA are reported in the Appendix A. They show that there is a statistically significant difference between the means of the groups for the dependent variable compression loads. The technique (S-SQ, S-ST, S-BT, D-SQ, D-ST, D-BT) has a statistically
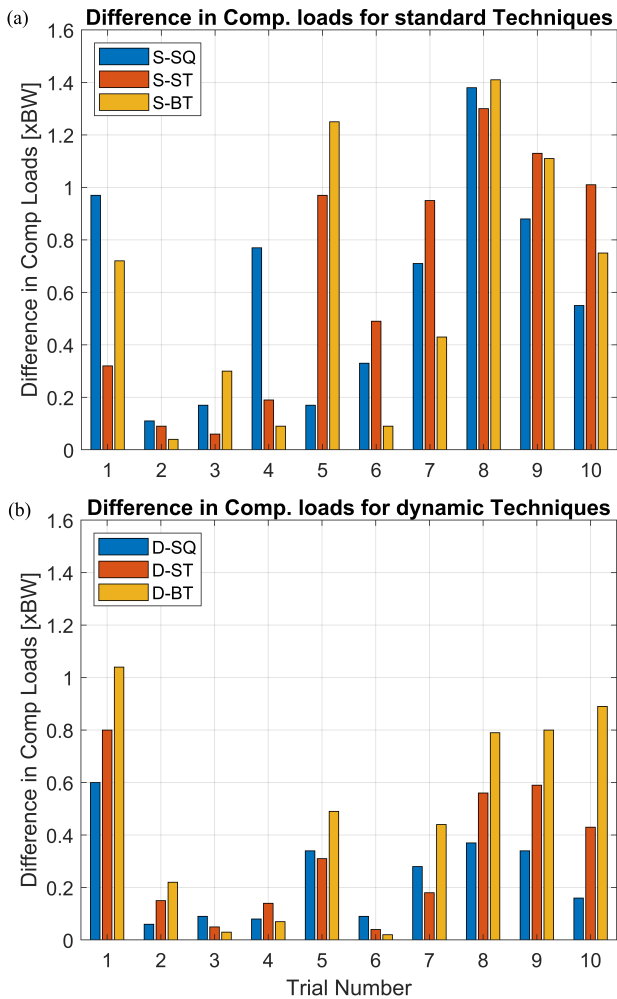
Fig. 7: Difference between L5-S1 peak compression loads estimations with marker-less and marker-based approach for static (a), dynamic (b) techniques

significant effect on the compression loads, while the method (marker-less, marker-based) variable does not. The interaction between the method variable and the technique variable is not statistically significant.

E. Other results

Average results for normalized EMG envelopes of a representative subject can be found in the appendix B.

IV. DISCUSSION

The aim and scope of this project was to design and test a marker-less approach to compute L5-S1 joint compression loads during dynamic lifting activities with a musculoskeletal model. This was evaluated by comparing the compression loads obtained from the marker-less approach and the ones obtained by the marker-based approach. Participants performed static and dynamic squats, stoops, and bilateral twists while lifting a 5kg dumbbell.

This project validated the marker-less workflow only for flexion/extension, despite OpenSim's LFB model allowing for analysis in three degrees of freedom (DoF).

Inverse kinematics results (Figure 4) showed that while marker-less data may have slightly higher variability, it still provides accurate information about the timing and overall patterns of movement, making it a viable alternative to marker-based methods. It is important to note that at the beginning of each task, participants had to move slightly forward and backward to synchronize the marker-based and marker-less systems. This initial movement may have caused the variability within gathered data. Despite this, the L5-S1 flexion-extension angle's amplitude and overall patterns align with reported values in existing literature [30], indicating that the range of motion captured by both the marker-based and marker-less systems is normal.

Figure 4 that there is a small phase shift between the marker-less and marker-based approaches, particularly in peaks and troughs. We hypothesize that this discrepancy may be attributed to the number of cluster markers used in the marker-less approach compared to the marker-based system. In the marker-less method, each limb is tracked using a single cluster marker, while the marker-based system employs three markers per limb. This discrepancy bears significance because the use of three markers defines a plane, ensuring precise limb orientation determination [31], whereas a lone marker only provides positional data. Employing three markers enables the capture of both rotational and translational movements, a crucial aspect for accurately modeling intricate human limb movements, especially in activities like squats, where high knee flexion exacerbates soft-tissue movement [32]. This hypothesis could be strengthened by delving deeper into the computed RMSE and R^2 values. Notably, the SQ technique exhibits the lowest R^2 values (0.520 and 0.541) for both static and dynamic experiments, accompanied by the highest RMSE values (0.682 and 0.593) within these categories These values suggest that the results obtained from the marker-less approach for the SQ technique significantly deviate from the actual observed values, implying considerable inaccuracies in the technique's estimations.

It is also important to consider that Nuitrack's tracking system operates focusing primarily on the front surface of the body. This means it can accurately identify and track keypoints visible from the front view. However, it lacks depth perception beyond this front-facing perspective. While it can pinpoint certain body parts like the clavicle, it may miss those obscured from its view, like the C7 vertebra. Hence, as detailed in section 2.A, it was imperative to gather supplementary measurements

from the subject to compute additional markers, albeit with less precision compared to the keypoints directly obtained from Nuitrack. Furthermore, since Nuitrack interprets visual data, factors such as lighting, movement velocity, distance from the sensor, and height can all introduce noise or ambiguity into the data, making it more challenging for the system to accurately track motion [1], [3], [4], [17], [19]. For instance, it was observed that when a subject was too tall and the Kinect didn't fully capture their head, Nuitrack attempted to locate the head of the person, resulting in a shift in the entire skeleton downwards. Additionally, it was noted that for dynamic activities, R^2 values were higher (0.92 and 0.939), and the RMSE values were lower (0.231 and 0.217). This was because as the subject moved forward, they were closer to the depth sensor, and the closer they were, the more accurate the gathered data became [33].

Inverse dynamics results, illustrated in Figure 5, also showed minor phase shifts between the marker-less and marker-based approaches. Yet, the curves align closely, especially in dynamic conditions. The obtained torque values fall within the range to those obtained in other studies under similar weight conditions [30], [34], [35]. Across all experimental trials, ST technique resulted in higher L5-S1 torques compared to SQ technique, as depicted in Figure 5. These results align with reported values in existing literature that reported that lifting techniques induce greater L5-S1 torques compared to squat [36].

Figure 6 demonstrates that compression load results show minor phase shifts between the marker-less and marker-based approaches. Overall, the curves align closely, especially in dynamic conditions. When compared to IK results, the RMSE values obtained for compression loads are lower, suggesting that the marker-less approach provides a better fit to the marker-based approach. However, there is also a decrease in R^2 values, indicating that the overall variance explained by the model has decreased. It is hypothesized that this could be due to the integration of EMG data to compute muscle forces. IK process is relatively straightforward yielding high R^2 values. It focuses on fitting joint angles to marker data by solving a least-squares problem that minimizes the differences between the measured marker locations and the model's virtual marker locations, subject to joint constraints [37]. On the other hand, computing muscle forces involves solving more complex dynamic equations. These computations consider muscle activations, force-length-velocity properties, and other biomechanical factors [15]. While these detailed computations can capture finer nuances of movement, improving the fit between both methods (as evidenced

by lower RMSE values), they also introduce noise and additional variability that were not present when considering kinematics alone. This highlights a trade-off: the model achieves a better fit (lower RMSE) at the cost of explaining less overall variance (lower R^2), due to the increased complexity and variability introduced by incorporating EMG data and more detailed biomechanical factors.

An ANOVA test was performed to evaluate if the differences between the marker-less and marker-based approaches in L5-S1 compression loads are statistically significant. The analysis revealed that the technique used has a significant impact on the compression loads, suggesting it is a key factor in determining the variance observed in the results. This indicates that variations in technique can lead to meaningful differences in L5-S1 compression loads. On the other hand, the method applied did not show a statistically significant effect, indicating that changes in the method do not lead to notable differences in compression loads. Additionally, the interaction between method and technique was not significant, implying that the combination of these factors does not influence the compression loads significantly. Therefore, it can be concluded that the specific technique used is a crucial factor in influencing L5-S1 compression loads, while the method and its interaction with the technique do not play a significant role.

Overall, the marker less approach allows the analysis of dynamic movements and accommodates to individual differences, providing more precise and personalized analyses than the NIOSH lifting model, which relies on generalized factors. This non-invasive method avoids the risks associated with sensor-based techniques. Unlike MTSs, which are accurate but confined to specialized laboratories and involve laborious setups, our marker less system enables motion capture in natural settings. This reduces setup time and minimizes artifacts from skin movement, enhancing the feasibility and comfort of motion analysis.

However, our study has a few limitations that are worth mentioning, with one significant concern being the lack of control over lifting speed. Consequently, different stages of lifting were not synchronized across repetitions, hindering the analysis of how speed influences motion tracking using the Kinect. Future research within this limitation could involve implementing controlled speed protocols to precisely examine the impact of lifting speed on motion tracking accuracy.

Another limitation pertained to the evaluation of only one weight or object. In industrial settings, workers often lift objects of various sizes and weights. Given that Nuitrack relies on visual data, it would have been crucial

to assess how objects obstructing different parts of the subject's body affect motion tracking. Future research could address this limitation by conducting experiments with a diverse range of objects, simulating not only real-world industrial activities but also scenarios. This could involve analyzing how objects of varying sizes and shapes impact motion tracking accuracy and developing algorithms to mitigate the effects of occlusion on tracking precision. For example, predictive modeling techniques could estimate the position of occluded joints based on visible body parts and prior motion patterns. Additionally, machine learning techniques, like training convolutional neural networks (CNNs) with datasets of occluded and non-occluded poses, could enhance the system's ability to predict hidden body parts accurately.

Additionally, the study solely focused on subjects facing the camera, neglecting movements such as turning and walking in the opposite direction, where only the subject's back is visible to the camera. And, due to time constraints, only flexion and extension movements were considered, overlooking other degrees of freedom (DOF) in motion analysis. Future research within this limitation could involve expanding the analysis to other DOF and walking in different directions.

Finally, future investigations could explore the efficacy of using three cluster markers per limb to enhance the accuracy and reliability of the marker-less approach in motion tracking systems. This could lead to improvements in tracking precision, especially in scenarios involving complex movements or occluded body parts by objects.

By rectifying the limitations noted, future progress in motion tracking technology might pave the way for the creation of tailored, resilient systems designed for industrial settings. These systems could enable early identification of improper lifting techniques or other workplace injury risks. Improved motion tracking precision could consequently foster safer workplaces and diminish occupational hazards for industrial workers.

V. Conclusions

This research has successfully proposed a new marker-less approach to compute L5/S1 joint compression loads during dynamic lifting activities using a musculoskeletal model. The proposed approach has been tested for several lifting techniques relevant to manual material handling industries. Results indicate a strong correlation between the marker-less and marker-based methods, particularly in dynamic conditions, validating the marker-less approach as a viable alternative. Additionally, the inclusion of muscle force estimations using CEINMS contributed to the accuracy of the compression load

calculations, highlighting the importance of considering muscle forces in movement analysis. This method offers a more flexible and less intrusive option for motion analysis, with potential applications in improving workplace safety.

VI. AI use

"During the preparation of this work the author(s) used ChatGPT, Copilot and Gemini for spelling and grammar checking. After using this tools, the author(s) reviewed and edited the content as needed and take(s) full responsibility for the content of the work."

References

[1] R. Mehrizi, X. Xu, S. Zhang, V. Pavlovic, D. Metaxas, and K. Li, "Using a marker-less method for estimating l5/s1 moments during symmetrical lifting," *Applied Ergonomics*, vol. 65, pp. 541–550, 2017. [Online]. Available: https://www.sciencedirect.com/science/article/pii/S0003687017300133

[2] S. Madinei, M. M. Alemi, S. Kim, D. Srinivasan, and M. A. Nussbaum, "Biomechanical assessment of two back-support exoskeletons in symmetric and asymmetric repetitive lifting with moderate postural demands," *Applied Ergonomics*, vol. 88, p. 103156, 2020. [Online]. Available: https://www.sciencedirect.com/science/article/pii/S0003687020301113

[3] "A computer-vision method to estimate joint angles and l5/s1 moments during lifting tasks through a single camera," *Journal of Biomechanics*, vol. 129, p. 110860, 2021. [Online]. Available: https://www.sciencedirect.com/science/article/pii/S0021929021006175

[4] H. Wang, Z. Xie, L. Lu, L. Li, X. Xu, and E. P. Fitts, "A single-camera computer vision-based method for 3d l5/s1 momentestimation during lifting tasks," *Proceedings of the Human Factors and Ergonomics Society Annual Meeting*, vol. 65, no. 1, pp. 472–476, 2021. [Online]. Available: https://doi.org/10.1177/1071181321651065

[5] C. Brandl, O. Brunner, P. Marzaroli, T. Hellig, L. Johnen, A. Mertens, M. Tarabini, and V. Nitsch, "Using real-time feedback of l5/s1 compression force based on markerless optical motion capture to improve the lifting technique in manual materials handling," *International Journal of Industrial Ergonomics*, vol. 91, p. 103350, 2022. [Online]. Available: https://www.sciencedirect.com/science/article/pii/S0169814122000919

[6] S. J. M. BIGOS, D. M. M. SPENGLER, N. A. B. MARTIN, J. P. ZEH, L. P. FISHER, A. M. NACHEMSON, and M. H. M. WANG, "Back injuries in industry: A retrospective study ii. injury factors," *spine*, vol. 11, no. 3, pp. 246–251, 1986. [Online]. Available: https://journals.lww.com/spinejournal/abstract/1986/04000/back_injuries_in_industry__a_retrospective_study_.11.aspx

[7] P.-L. Liu, C.-C. Chang, H.-Y. Kao, and C.-Y. Hsiao, "Artificial neural network can improve the accuracy of a markerless skeletal model in l5/s1 position estimation during symmetric lifting," *Journal of Biomechanics*, vol. 130, p. 110844, 2022. [Online]. Available: https://www.sciencedirect.com/science/article/pii/S0021929021006035

[8] X. Xu and R. W. McGorry, "The validity of the first and second generation microsoft kinect™ for identifying joint center locations during static postures," *Applied Ergonomics*, vol. 49, pp. 47–54, 2015. [Online]. Available: https://www.sciencedirect.com/science/article/pii/S0003687015000149

[9] J. Wang, J. Chu, J. Song, and Z. Li, "The application of impantable sensors in the musculoskeletal system: a review," *Frontiers in Bioengineering and Biotechnology*, vol. 12, 2024. [Online]. Available: https://www.frontiersin.org/articles/10.3389/fbioe.2024.1270237

[10] J. W. Fernandez and M. G. Pandy, "Integrating modelling and experiments to assess dynamic musculoskeletal function in humans," *Experimental Physiology*, vol. 91, no. 2, pp. 371–382. [Online]. Available: https://physoc.onlinelibrary.wiley.com/doi/abs/10.1113/expphysiol.2005.031047

[11] S. L. Delp, F. C. Anderson, A. S. Arnold, P. Loan, A. Habib, C. T. John, E. Guendelman, and D. G. Thelen, "Opensim: Open-source software to create and analyze dynamic simulations of movement," *IEEE Transactions on Biomedical Engineering*, vol. 54, no. 11, pp. 1940–1950, 2007.

[12] S. C. E. B. R. F. B. J. C. F. R. B. G. D. T. Erica Beaucage-Gauvreau, William S. P. Robertson and C. F. Jones, "Validation of an opensim full-body model with detailed lumbar spine for estimating lower lumbar spine loads during symmetric and asymmetric lifting tasks," *Computer Methods in Biomechanics and Biomedical Engineering*, vol. 22, no. 5, pp. 451–464, 2019, pMID: 30714401. [Online]. Available: https://doi.org/10.1080/10255842.2018.1564819

[13] N. J. Jarque-Bou, J. L. Sancho-Bru, and M. Vergara, "A systematic review of emg applications for the characterization of forearm and hand muscle activity during activities of daily living: Results, challenges, and open issues," *Sensors*, vol. 21, no. 9, 2021. [Online]. Available: https://www.mdpi.com/1424-8220/21/9/3035

[14] J. A. Zellers, S. Parker, A. Marmon, and K. Grävare Silbernagel, "Muscle activation during maximum voluntary contraction and m-wave related in healthy but not in injured conditions: Implications when normalizing electromyography," *Clinical Biomechanics*, vol. 69, pp. 104–108, 2019. [Online]. Available: https://www.sciencedirect.com/science/article/pii/S026800331830980X

[15] C. Pizzolato, D. G. Lloyd, M. Sartori, E. Ceseracciu, T. F. Besier, B. J. Fregly, and M. Reggiani, "Ceinms: A toolbox to investigate the influence of different neural control solutions on the prediction of muscle excitation and joint moments during dynamic motor tasks," *Journal of Biomechanics*, vol. 48, no. 14, pp. 3929–3936, 2015. [Online]. Available: https://www.sciencedirect.com/science/article/pii/S0021929015005151

[16] d. P. O. T. . N. J. Das, K., "Comparison of markerless and marker-based motion capture systems using 95

[17] D. Pagnon, M. Domalain, and L. Reveret, "Pose2sim: An end-to-end workflow for 3d markerless sports kinematics—part 2: Accuracy," *Sensors*, vol. 22, no. 7, 2022. [Online]. Available: https://www.mdpi.com/1424-8220/22/7/2712

[18] H. Tsushima, M. E. Morris, and J. McGinley, "Test-retest reliability and inter-tester reliability of kinematic data from a three-dimensional gait analysis system," *Journal of the Japanese Physical Therapy Association*, vol. 6, no. 1, pp. 9–17, 2003.

[19] D. Pagnon, M. Domalain, and L. Reveret, "Pose2sim: An end-to-end workflow for 3d markerless sports kinematics—part 1: Robustness," *Sensors*, vol. 21, no. 19, 2021. [Online]. Available: https://www.mdpi.com/1424-8220/21/19/6530

[20] N. Ahmad, R. A. B. R. Ghazilla, N. M. Khairi, and V. Kasi, "Reviews on various inertial measurement unit (imu) sensor applications," in *IEEE Workshop on Signal Processing Systems*, 2013. [Online]. Available: https://api.semanticscholar.org/CorpusID:8798242

[21] G. Thomas, R. Gade, T. B. Moeslund, P. Carr, and A. Hilton, "Computer vision for sports: Current applications and research topics," *Computer Vision and Image Understanding*, vol. 159, pp. 3–18, 2017, computer Vision in Sports.

[Online]. Available: https://www.sciencedirect.com/science/article/pii/S1077314217300711

[22] F. Asadi and N. Arjmand, "Marker-less versus marker-based driven musculoskeletal models of the spine during static load-handling activities," *Journal of Biomechanics*, vol. 112, p. 110043, 2020. [Online]. Available: https://www.sciencedirect.com/science/article/pii/S002192902030467X

[23] Z. Cao, G. Hidalgo, T. Simon, S.-E. Wei, and Y. Sheikh, "Openpose: Realtime multi-person 2d pose estimation using part affinity fields," *IEEE Transactions on Pattern Analysis and Machine Intelligence*, vol. 43, no. 1, pp. 172–186, 2021.

[24] Z. Cao, T. Simon, S.-E. Wei, and Y. Sheikh, "Realtime multi-person 2d pose estimation using part affinity fields," in *Proceedings of the IEEE Conference on Computer Vision and Pattern Recognition (CVPR)*, July 2017.

[25] F. Bailly, A. Ceglia, B. Michaud, D. M. Rouleau, and M. Begon, "Real-time and dynamically consistent estimation of muscle forces using a moving horizon emg-marker tracking algorithm—application to upper limb biomechanics," *Frontiers in Bioengineering and Biotechnology*, vol. 9, 2021. [Online]. Available: https://www.frontiersin.org/articles/10.3389/fbioe.2021.642742

[26] A. Moya-Esteban, H. van der Kooij, and M. Sartori, "Robust estimation of lumbar joint forces in symmetric and asymmetric lifting tasks via large-scale electromyography-driven musculoskeletal models," *Journal of Biomechanics*, vol. 144, p. 111307, 2022. [Online]. Available: https://www.sciencedirect.com/science/article/pii/S0021929022003487

[27] M. Rajaee, N. Arjmand, and A. Shirazi-Adl, "A novel coupled musculoskeletal finite element model of the spine–critical evaluation of trunk models in some tasks," *Journal of Biomechanics*, vol. 119, p. 110331, 2021.

[28] N. Arjmand, A. Plamondon, A. Shirazi-Adl, C. Lariviere, and M. Parnianpour, "Predictive equations to estimate spinal loads in symmetric lifting tasks," *Journal of biomechanics*, vol. 44, no. 1, pp. 84–91, 2011.

[29] D. Chicco, M. J. Warrens, and G. Jurman, "The coefficient of determination r-squared is more informative than smape, mae, mape, mse and rmse in regression analysis evaluation," *Peerj computer science*, vol. 7, p. e623, 2021.

[30] "Electromyography-driven musculoskeletal models with time-varying fatigue dynamics improve lumbosacral joint moments during lifting," *Journal of Biomechanics*, vol. 164, p. 111987, 2024. [Online]. Available: https://www.sciencedirect.com/science/article/pii/S0021929024000642

[31] L. Carcreff, G. Payen, G. Grouvel, F. Massé, and S. Armand, "Three-dimensional lower-limb kinematics from accelerometers and gyroscopes with simple and minimal functional calibration tasks: Validation on asymptomatic participants," *Sensors*, vol. 22, no. 15, 2022. [Online]. Available: https://www.mdpi.com/1424-8220/22/15/5657

[32] J. M. Buchman-Pearle and S. M. Acker, "Estimating soft tissue artifact of the thigh in high knee flexion tasks using optical motion capture: Implications for marker cluster placement," *Journal of Biomechanics*, vol. 127, p. 110659, 2021. [Online]. Available: https://www.sciencedirect.com/science/article/pii/S0021929021004280

[33] K. Khoshelham and S. O. Elberink, "Accuracy and resolution of kinect depth data for indoor mapping applications," *Sensors*, vol. 12, no. 2, pp. 1437–1454, 2012. [Online]. Available: https://www.mdpi.com/1424-8220/12/2/1437

[34] I. Kingma, C. T. Baten, P. Dolan, H. M. Toussaint, J. H. van Dieën, M. P. de Looze, and M. A. Adams, "Lumbar loading during lifting: a comparative study of three measurement techniques," *Journal of Electromyography and Kinesiology*, vol. 11, no. 5, pp. 337–345, 2001. [Online]. Available: https://www.sciencedirect.com/science/article/pii/S1050641101000116

[35] A. Moya-Esteban, N. P. Brouwer, A. Tabasi, H. v. d. Kooij, I. Kingma, and M. Sartori, "Muscle-level analysis of trunk mechanics via musculoskeletal modeling and high-density electromyograms," in *2020 8th IEEE RAS/EMBS International Conference for Biomedical Robotics and Biomechatronics (BioRob)*, 2020, pp. 1109–1114.

[36] M. Abdoli-E, M. J. Agnew, and J. M. Stevenson, "An on-body personal lift augmentation device (plad) reduces emg amplitude of erector spinae during lifting tasks," *Clinical Biomechanics*, vol. 21, no. 5, pp. 456–465, 2006. [Online]. Available: https://www.sciencedirect.com/science/article/pii/S0268003306000064

[37] S. L. Delp, F. C. Anderson, A. S. Arnold, P. Loan, A. Habib, C. T. John, E. Guendelman, and D. G. Thelen, "Opensim: Open-source software to create and analyze dynamic simulations of movement," *IEEE Transactions on Biomedical Engineering*, vol. 54, no. 11, pp. 1940–1950, 2007.

APPENDIX

A. ANOVA TEST

Results of ANOVA for all lifting techniques can be seen in figure A.1. The peak compression loads were considered to be the dependent variable. Factors such as the lifting method (S-SQ, S-ST, S-BT, W-SQ, W-ST, W-BT) and the estimation method (marker-less, marker-based) were considered as independent factors. The effect of independent factors along with their interaction effects on the dependent variable were studied using ANOVA with alpha=0.05.

Tests of Between-Subjects Effects

Dependent Variable: comploads

Source	Type III Sum of Squares	df	Mean Square	F	Sig.	Partial Eta Squared
Corrected Model	60.741[a]	11	5.522	2.809	.003	.222
Intercept	2904.670	1	2904.670	1477.715	<.001	.932
method	.668	1	.668	.340	.561	.003
technique	59.778	5	11.956	6.082	<.001	.220
method * technique	.295	5	.059	.030	1.000	.001
Error	212.290	108	1.966			
Total	3177.701	120				
Corrected Total	273.031	119				

Fig. A.1: Peak compression loads ANOVA results performed in SPSS

B. EMG normalized envelopes

Figure B.1 shows all the obtained normalized EMG envelopes of a representative subject for all lifting conditions.
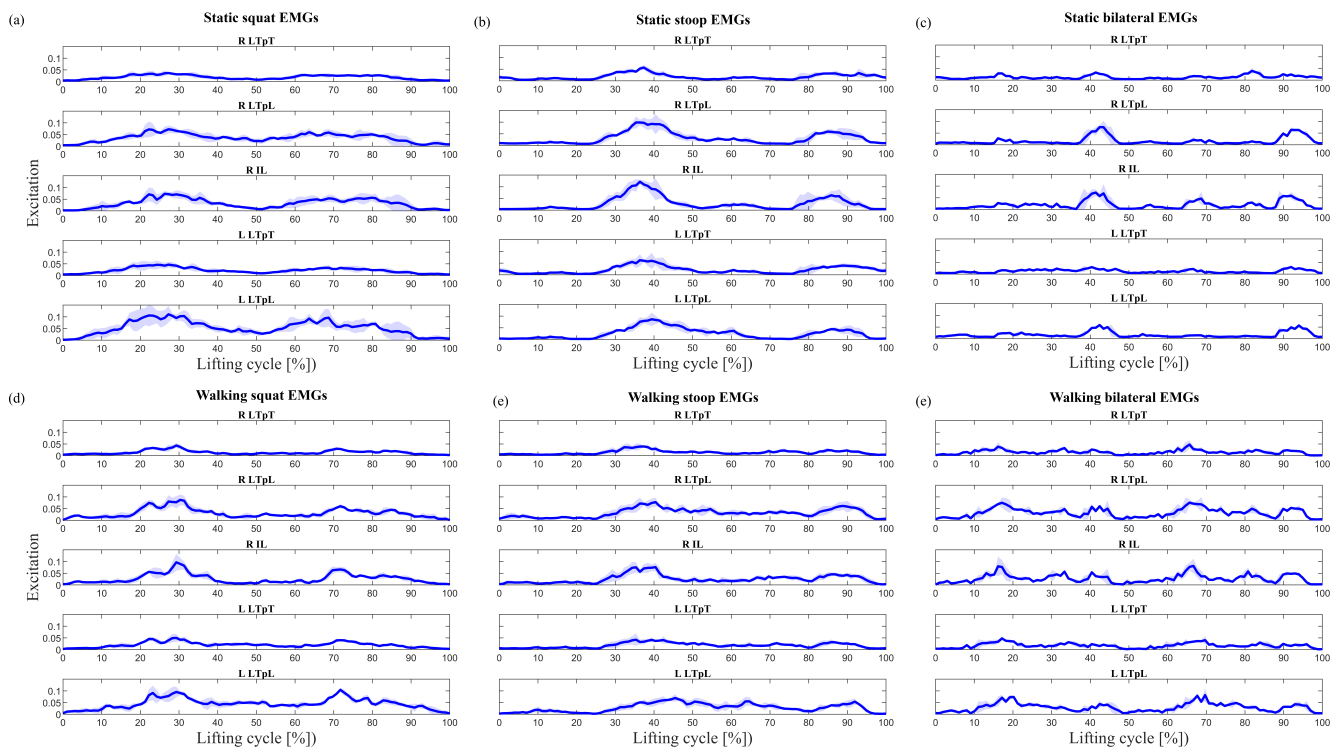

Fig. B.1: Normalized EMG envelopes of a representative participant (subject 9) for the right IL and left/right LTpL and LTpT muscles. Plot show the results for several lifting techniques with a 5 kg dumbbell. The techniques include S-SQ (a), S-ST (b), S-BT (c), D-SQ (d), D-ST (e), and D-BT (f). Solid line represents the mean and shaded region the standard deviation